ELSEVIER

International Journal of Pharmaceutics 127 (1996) 219–227

international journal of pharmaceutics

An analysis of the Fraunhofer Diffraction method for particle size distribution analysis and its application to aerosolized sprays

Ananth Annapragada*, Akwete Adjei

Abbott Laboratories, Pharmaceutical Products Division, North Chicago, IL 60064, USA

Received 27 March 1995; revised 11 July 1995; accepted 17 July 1995

Abstract

The Fraunhofer Diffraction technique is used widely for particle sizing applications in the 1–200 μm size range. The technique is suitable for use with liquid-borne and gas-borne suspensions, and is therefore well suited for use in the characterization of aerosol dosage forms. While the theory relating to Fraunhofer Diffraction and the determination of particle sizes from the diffraction patterns has been fairly well worked out, there is little quantitative information in the literature on the extent of variability, the accuracy and the precision to expect in the measurements. This work therefore addresses the nature and magnitude of errors in determining size distributions by the Fraunhofer Diffraction technique. The diffraction patterns to be expected from known particle size distributions are calculated from first principles and compared with experimental data acquired on a commercial Fraunhofer instrument. Known noise levels are imposed on the simulated data in order to approximate experimental conditions. These noisy data sets are then inverted by a minimization procedure to yield particle size distributions which can be compared with the distributions used to simulate the data in the first place. This comparison provides information on the errors and variability to be expected in such measurements under a variety of controlled experimental conditions and allows us to assign error limits to measurements made using the Fraunhofer technique. The report thus provides a mathematical basis for setting reasonable particle size specifications as a way of quantitative assessment of product performance in vitro.

1. Introduction

The Malvern 2600 Size Analyzer is used to determine particle size distributions in the 1–200 μm size range. The instrument operates using the principles of Fraunhofer Diffraction Pattern Analysis (FDPA). The technique was first introduced by Swithenbank et al., 1977. A number of researchers have reviewed the technique (Bayvel and Jones, 1981; Hirleman et al., 1984; Gulari et al., 1985). In FDPA, a laser beam is collimated to a diameter of a few millimeters, and passed through a sample. The sample is typically a liquid or gas suspension of the particles whose size distribution is to be determined. The laser energy is scattered by the particles and results in a characteristic energy distribution at small angles of

* Corresponding author.

SSDI 0378-5173(95)04217-X

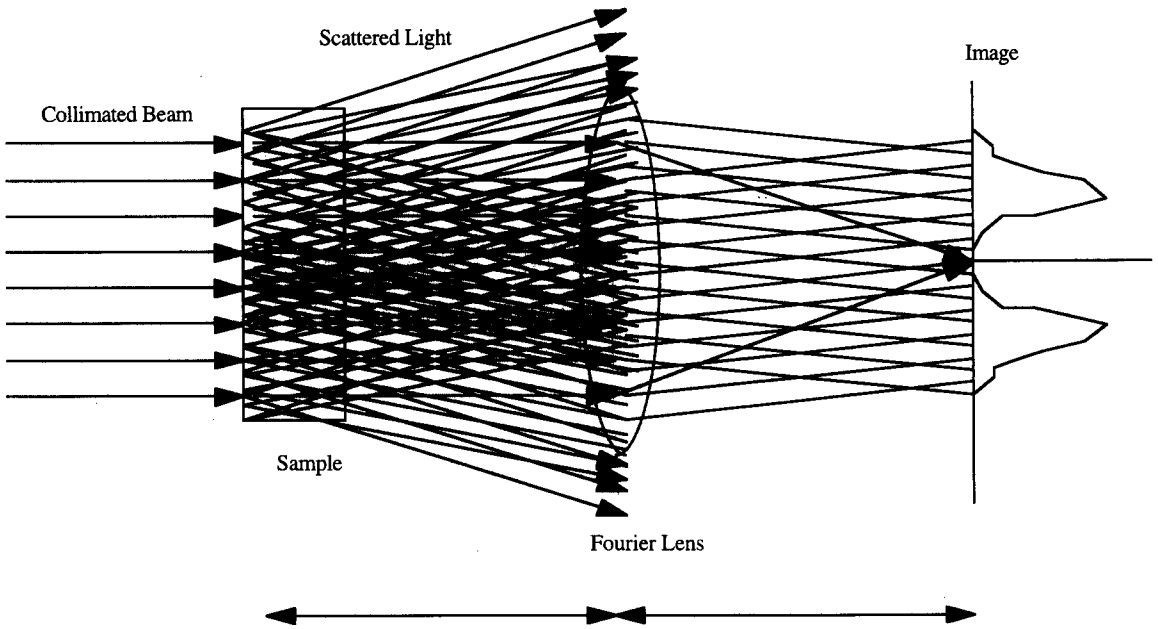

Fig. 1. Typical Fraunhofer Diffraction setup.

deviation from the forward beam. A portion of this pattern is focused by a lens of known focal length onto a detector. In the Malvern instrument, the detector consists of a series of concentric photo detector rings. The detector response is averaged over some period of time and recorded. Size distributions are then determined by numerically inverting the recorded pattern.

2. Theory

Fig. 1 shows a schematic of a typical FDPA experiment. For a monodisperse system of spherical particles in the sample which are larger than the wavelength of the light used, the diffraction pattern would be described (following the nomenclature of Hirleman et al., 1984 by the characteristic Airy diffraction equation:

$$I(\theta) = I_0 \int_0^\infty \frac{\prod^2 D^4}{16\lambda^2} \left[\frac{2J_1\left(\frac{\pi D\theta}{\lambda}\right)}{\frac{\pi D\theta}{\lambda}} \right]^2 n(D)dD \qquad (1)$$

$I(\theta)$ is the scattered intensity at any angle θ, $I < \mathrm{INF} > 0 < /\mathrm{INF} >$ the incident intensity, λ the wavelength of the incident light, D the diameter of particles in the sample, and $n(d)$ the particle size (number) distribution.

This pattern is then refracted by a transform lens (of finite aperture) onto a detector of finite diameter. Neglecting the aberrations due to finite aperture, the transformed pattern can be obtained by the following transformation:

$$r = f\theta \qquad (2)$$

where f is the focal length of the lens and r the radial position in the pattern.

The energy within any detector element of inner radius s_1 and outer radius s_2 is then given by:

$$E(s_1,s_2) = \int_0^\infty A(D)[(J_0^2 + J_1^2)|_{s_1} - (J_0^2 + J_1^2)|_{s_2}] \times dD \qquad (3)$$

where

$$J_n|_{s_1} = J_n\left(\frac{\pi D s_i}{\lambda}\right) \qquad (4)$$

is the Bessel function of the nth order and first kind with argument $\frac{\pi D s_i}{\lambda}$, and $A(D)$ is the area fraction distribution of the particles in the system. Note the change from the number fraction distribution in the original Airy equation (Eq. (1)).

The detector elements each exhibit a response which is assumed to be proportional to the incident energy. The response (normally a voltage or a current, depending on the energizing and analysis circuitry) is then given by:

$$V(s_1,s_2) = c'(s_1,s_2)E(s_1,s_2) \tag{5}$$

where c' is a proportionality constant. Older instruments have assumed that the proportionality (or calibration) constant is invariant for all the detector elements. However, variations of up to $\pm$ 30% have been reported by Hirleman et al. (1984) and hence c' is shown here as a function of s_1 and s_2. In the present generation of Malvern instruments (2600 and MasterSizer), each individual instrument is specifically calibrated and the values of the array c' are stored on the computer associated with the instrument and used for the calculations. Other vendors store the calibration constants on a ROM chip on the instrument itself.

3. Calculating the size distribution: inversion of the diffraction pattern

Several methods exist to calculate the size distribution from the detector response $V(s_1,s_2)$. In general, direct integral transform methods using Fast Fourier Transform (FFT) programs are fast and simple to implement but lack precision due to the poor spatial resolution of the detector array (Bayvel and Jones, 1981). The methods used most commonly are as follows.

(1) Model dependent

◆Assume a model such as Log-Normal or Rosin-Rammler for the size distribution.

◆ Simulate the detector response expected for this distribution.

◆ Optimize the model parameters by minimizing the sum of squared deviations from the measured detector response.

(2) Model independent

◆ Assume that the size distribution consists of a finite number of fixed size classes.

◆ Simulate the detector response expected for this distribution.

◆ Optimize the weight fractions in each size class by minimizing the sum of squared deviations from the measured detector response.

The models used in the model-dependent process are all unimodal. Therefore, the utility of the model-dependent inversion technique is limited to systems which are definitely unimodal and known to follow one of the commonly used models of particle size distribution. The efficacy of the model-dependent approach in characterizing unimodal distributions has already been proven in the literature (Hirleman et al., 1984).

The more general case of multimodal distributions is best approached by the model independent method of analysis which makes no such assumptions. However, the number of available detector channels also limits the number of size classes which can be included in the model-independent analyses. For the Malvern machines, this is normally 32 classes. Since the model-independent method is the most general method of measuring size distributions, it is the focus of this work.

For a finite number of size classes m, Eq. (6) can be written as:

$$\frac{E}{c'}\Big|_{s_1,s_2} = \sum_{i=1}^{m} N_i[(J_0^2 + J_1^2)|_{s_1} - (J_0^2 + J_1^2)|_{s_2}] \tag{6}$$

where the J values are Bessel functions of the first kind as defined earlier.

The corresponding detector responses $V(s_1,s_2)$ are measured experimentally by averaging for a finite time. For a system with N detector rings, N equations can be written as follows:

$$\delta_j = V_j - \sum_{i=1}^{m} N_i[(J_0^2 + J_1^2)|_{s_1} - (J_0^2 + J_1^2)|_{s_2}] \tag{7}$$

A solution to the system (6) can then be obtained by minimizing

$$R = \sum_{j=1}^{N} \delta^2 \tag{8}$$

by some numerical minimization technique such as the Marquardt-Levenberg algorithm.

Since only N equations are present in (7), the minimization of R can only be done in N-space. Therefore, in order to successfully invert the diffraction pattern and obtain the size distribution, the entire distribution has to be represented with a maximum of N parameters. For a model-independent calculation therefore, one is limited to $\frac{N}{2}$ radii and $\frac{N}{2}$ number densities at these radii. Alternatively, the radii can be fixed for a given analysis and the entire set of N variables can be dedicated to N number-densities. This is the method used in the Malvern machines.

4. Sources of error in determination of size distributions

The following are possible sources of error while determining the size distribution:(1) Random noise at the sensitivity limit of the detector elements.(2) Inappropriate assignment of radii to cover the size distribution, or presence of particles outside the assigned range of radii.(3) Insufficient number of detector elements to appropriately resolve a multimodal size distribution(4) Dependencies on the convergence algorithm: starting points, convergence criteria and discretization of the distribution.

A number of equipment vendors use the same detector element: a 31-ring concentric detector which is used in the Malvern machines. Therefore, these instruments are essentially identical in performance under the first three categories above. However, each vendor has their own data-fit algorithm, and therefore under category 4 above, the performance is unique and individual. Since the exact nature of the algorithms is not available to the public, and is not revealed by the vendors, it is not possible to evaluate the effect of this factor for all instruments. In the case of the Malvern 2600 however, the software allows access to the inversion algorithm as a stand-alone block. In this study therefore, the Malvern 2600 is used to represent a 'typical' Fraunhofer instrument. Under the categories 1–3 above, all 31-ring instruments should have similar performance, while under category 4, the Malvern can be considered representative of the class, but not necessarily the same in performance as a 31-ring machine from a different vendor. Other manufacturers of FDPA instruments utilize higher resolution detectors, and modified optics. These are the subject of a future paper.

In order to evaluate the magnitude of errors to be expected due to each of these factors, the following approach is used: (1) Simulate diffraction patterns for known size distributions.(2) Superimpose random noise on the pattern commensurate with the detection emits of the detector elements.(3) Invert the patterns by the same minimization technique used by the Malvern instruments.(4) Compare the inverted patterns with the known size distribution and check for quantitative correctness.

5. Observations and conclusions

The calibration constants for each of the 31 rings in the detector element are stored by the Malvern machine on the same disk where the control software is located. Alternately, the calibration factors can be calculated by the procedure of Hirleman et al., 1984. Using these calibration factors, we are in a position to accurately model the diffraction patterns resulting from Airy Fraunhofer regime particles when analyzed by the Malvern 2600 machine.

Fig. 2 shows the size distributions calculated by inverting the simulated scattering patterns of 1 and 10 μm particles at various noise levels. It is apparent that for narrow unimodal systems such as these, the inversion algorithm is insensitive to noise, and is accurate in its measurement of particle size. The only error in the estimation of diameter is limited to the width of the bars (size ranges) used in the computation.

Fig. 3 shows the size distributions calculated by inverting the simulated scattering patterns of a 1–3 μm bimodal system at increasing noise levels. It is apparent that the 1 μm peak is not visible by the Fraunhofer technique. While 1 μm is at the manufacturer-declared lower limit for the ma-

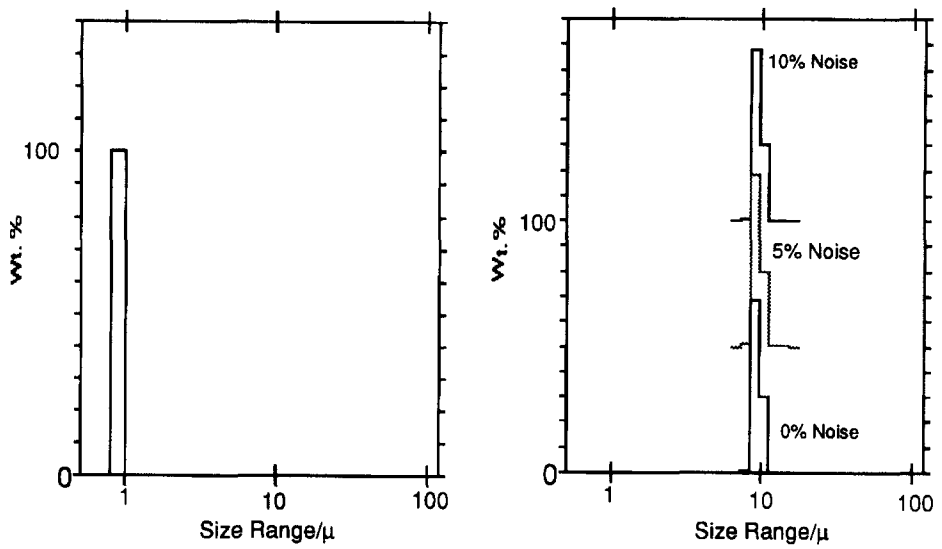

Fig. 2. Size distributions calculated by inverting the scattering signatures of 1-μm and 10-μm particles at various noise levels.

chine, a size bar for < 1.2 μm exists in the size spectrum, and is populated completely when a monodisperse system is analyzed. Therefore, a detection limit for 1 μm particles in a 1–3 μm system must exist. In order to probe this limit, a number of scattering patterns were generated for 1–3 μm systems of varying relative concentrations of 1-μm to 3-μm particles. The size distributions estimated by Malvern inversion of the scattering patterns are plotted in Fig. 4. From these data, it is possible to plot the theoretical and measured mass fractions of 1-μm and 3-μm particles in a phase-diagram format as in Fig. 5. The deviation from the diagonal straight lines is an indication of the magnitude of the error to be expected in estimating mass fractions in a bimodal 1–3 μm mixture at any given concentration. For example, at 50% mass fraction 1-μm particles, the dominant peak in the fitted size distribution is the 3 μm peak, while at 62% mass fraction 1-μm particles, the measurement is much more accurate. At higher than 62% again, the sensitivity lapses to

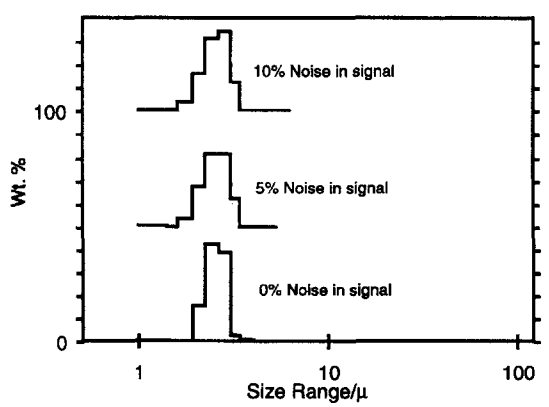

Fig. 3. Size distributions calculated by inverting the scattering patterns of 1 μm/3 μm particles at increasing noise levels.

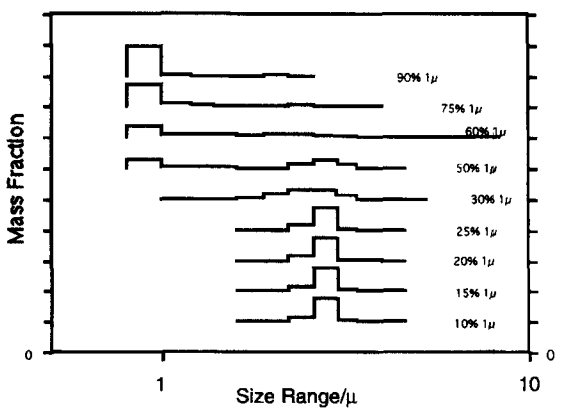

Fig. 4. Size distributions calculated by inverting scattering patterns for 1 μm/3 μm bimodal systems of varying relative concentration at a noise level of 5%.

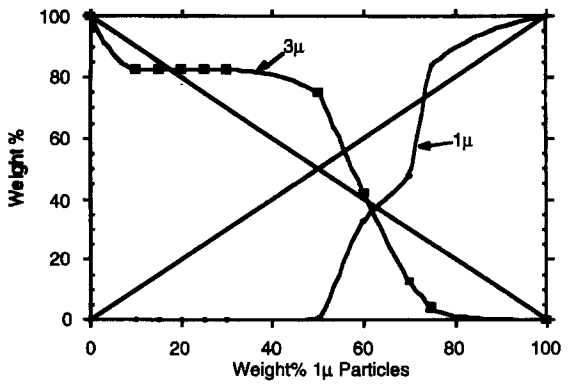

Fig. 5. Measured and actual weight fractions of 1-μm and 3-μm particles in theoretical mixtures of various relative concentration.

the opposite end of the spectrum, showing predominantly 1-μm particles at the expense of the 3 μm peak. Fig. 6 shows a similar phase diagram plot for the 1–10 μm system, showing a similar behaviour of deviation from the diagonals.

Fig. 7 shows the size distributions calculated by the Malvern program by inverting calculated scattering patterns of 1 μm–3 μm–10 μm trimodal mixtures with equal mass fractions in each of the three modes. Once again, the 1 μm mode is not present in the fitted distributions. A fairly significant noise-effect is also noticed where the mass fraction in the 10 μm band gets progressively lower with increasing noise level.

Fig. 8 shows the size distributions calculated by

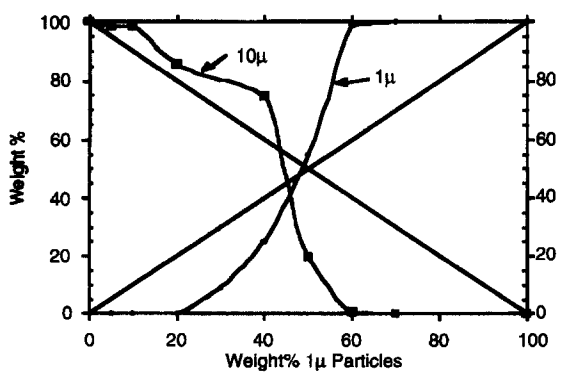

Fig. 6. Measured and actual weight fractions of 1-μm and 10-μm particles in theoretical mixtures of varying relative concentration.

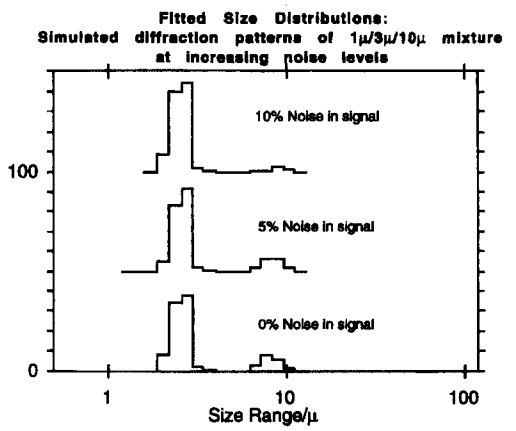

Fig. 7. Size distributions calculated by fitting scattering patterns of 1 μm/3 μm/10 μm particles in equal mass fractions at increasing noise levels.

fitting the scattering patterns of a 3 μm–10 μm–200 μm system of particles. The manufacturer-declared upper limit of size for the Malvern system using a 63 mm lens is 118.4 μm. This study therefore probes the effect of the presence of particles above the upper limit on the accuracy and precision of the measurement. The results show that while the 3-μm and 10-μm peaks are quantitatively correct, the 200-μm particles are not represented, even in the 'over 118.4 μm' category.

From the studies of simulated scattering patterns and their inversion, we can therefore conclude that while unimodal distributions are

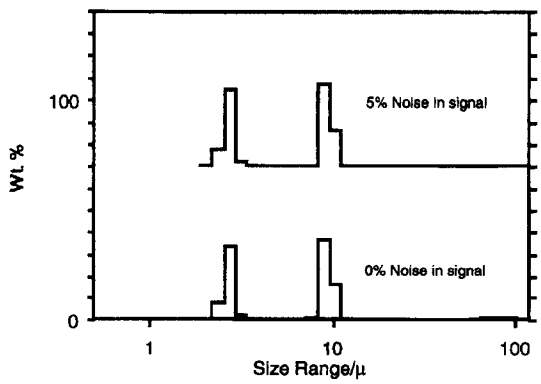

Fig. 8. Size distributions calcualted by fitting the scattering patterns of 3 μm/10 μm/200 μm particles in equal mass fractions at increasing noise levels.

Ring Pair	Residual
1 + 2	-3
3 + 4	-6
5 + 6	-9
7 + 8	-13
9+ 10	-14
11 + 12	-9
13 + 14	3
15 + 16	0
17 + 18	-112
19 + 20	-394
21 + 22	-473
23 + 24	-267
25 + 26	-819
27 + 28	-653
29 + 30	-806

Fig. 9. Table of residuals when a 10 μm simulated scattering pattern is fitted using the Malvern Model-independent program.

analyzed accurately, multimodal distributions are not necessarily well handled. The reasons for this may be ascertained by looking at the residuals at the best-fit as determined by the fitting program. Residuals from the fit of a 10 μm scattering pattern are shown in Fig. 9. Note that the residual is zero at the highest peak in the distribution and is larger everywhere else. While it is difficult to determine the reason for this without a knowledge of the algorithm used in the fitting program, it is possible to guess at the algorithm from these data. It appears that since the residual is zero at the highest peak and larger everywhere else, and that since most best-fit algorithms attempt to minimize the sum of squared residuals at all points, the fitting program must in some fashion weight the residual at the highest peak higher than everywhere else. Such a weighting will cause a distribution of residuals as seen in Fig. 9. The effect on the analysis of real data will be to skew the analysis to finding one major peak in the fitted size distribution, as seen in this work. Bimodal distributions will therefore be unfairly weighted in the analysis to one or the other mode in the distribution. This is precisely the behaviour observed in this work in the analysis of 1 μm–3 μm and 1 μm–10 μm bimodal systems.

The main goal of the manufacturing process for inhalation aerosols is to maximize the mass fraction of particles below 10 μm. It has been shown in other work that particles smaller than 10 μm have the highest probability of being delivered successfully to the deep lung. It is therefore of importance to know what level of particles of size greater than 10 μm will be visible in a particle system that is predominantly below 10 μm. Obviously, it will be useful if the distribution below 10 μm is representative of a typical inhalation aerosol material. In order to probe this sensitivity, a typical size distribution of manufactured aerosol particles was subjected to sensitivity analysis. Fig. 10 shows the size distributions calculated by inversion of the scattering patterns of distributions $<$ 10 μm with 50-μm particles spiked in at increasing levels. The same analysis can be performed for spikes of other particle sizes; Fig. 11 shows the size distributions calculated by inverting the scattering patterns of the same parent size distribution as in Fig. 10 with increasing fractions of a 20 μm spike. From the data in Figs. 10 and 11, it is possible to calculate the mass fractions above and below 10 μm as calculated by the Fraunhofer inversion method for each of the size distributions. This data are plotted in Fig. 12 in phase diagram format. If the Fraunhofer technique were perfect in determining mass fractions below and

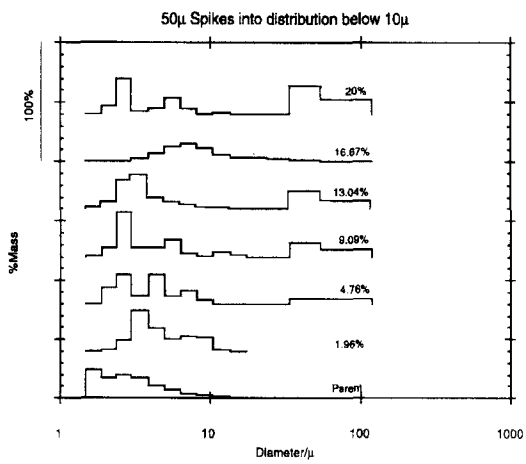

Fig. 10. Fitted size distributions from scattering patterns of size distributions with increasing mass fractions of 50-μm particles in a constant distribution of particles below 10 μm.

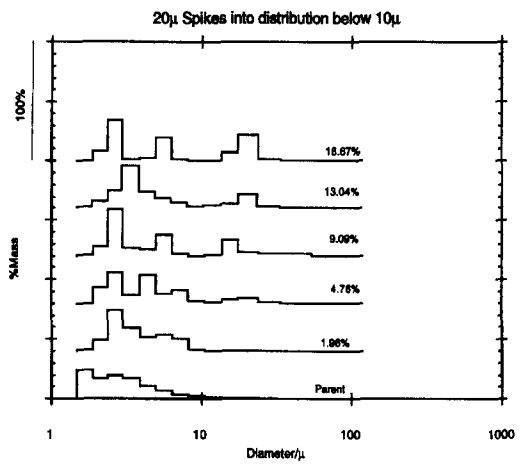

Fig. 11. Fitted size distributions from scattering patterns of size distributions with increasing mass fractions of 20-μm particles in a constant distribution of particles below 10 μm.

above the 10 μm cutoff, then all the data points should have collapsed onto the two solid lines ('theoretical $>$ 10 μm' and 'theoretical $<$ 10 μm'). The deviations from these two lines are a measure of the errors involved in the measurement. Note that the deviations are POSITIVE for $>$ 10-μm particle mass fractions of greater than 5%. Further, for $>$ 10-μm particle mass fractions of more than 7%, the measured mass fraction by the Fraunhofer method is more than 10%.

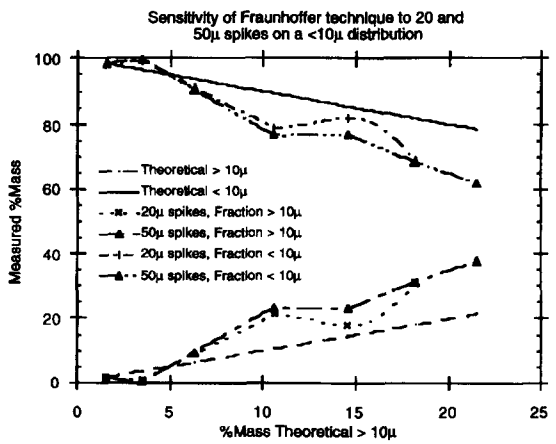

Fig. 12. Mass fractions below and above 10 μm as calculated by Malvern FDPA algorithm from calculated intensity distributions of particles below 10 μm spiked with increasing concentrations of 20 μm and 50 μm particles.

6. Conclusions

The Fraunhofer diffraction pattern analysis method of particle sizing works well for unimodal systems. For sharp-peaked multimodal systems, there is a strong tendency to skew the distribution towards the mode that contributes the strongest peak in the diffraction pattern. In the presence of small particles ($\leq$ 1 μm, just below the lower limit of the FDPA system), the modes of multimodal distributions can be assigned incorrect mass fractions. In the extreme case, modes can be missed completely, and not represented at all in the measured distributions. The same problem appears in the case of particle larger than the declared upper limit for the FDPA system; modes in a multimodal system, particularly the oversize particles, can be missed completely in the measured distribution. For broader multimodal distributions, with sizes completely within the declared limits of the FDPA system, the mass fraction predictions are also inaccurate, possibly by as much as 15% in a given mode (Figs. 5 and 6). It appears that so long as the concentration of particles below the lower limit of the range (1 μm) is low, the errors tend to exaggerate the mass fractions of large particles ($>$ 10 μm). However, when the small particle concentration increases, the measured concentrations of large particles fall below the actual concentrations.

It should also be noted that this behaviour is for the ideal case of hypothetical particles that exactly follow the Fraunhofer theory. In reality, particles could be non-spherical, and possess refractive indices that are close to that of the medium. The scattering pattern of these particles would then deviate further from the Fraunhofer prediction, and cause further errors.

The implications for inhalation aerosol particle characterization are therefore as follows: (1) If the product were predominantly unimodal in size distribution, with negligible concentrations outside the declared limit of the FDPA technique (1.2 μm to 118.4 μm for the 63 mm lens), the measured size distributions would be accurate. We would expect that this would be the normal case during manufacture.(2) If the product were multimodal with one or more modes of particles larger than

the upper limit on size (118.4 μm for the 63 mm lens) present, the measured sized distribution would be inaccurate; typically the particles outside the upper limit will be completely missing from the measured distribution. In some cases, if the oversize mode is close to the upper limit, a mode will appear in the uppermost size fraction. This should be an indication to use a longer focal length lens and re-analyze the sample.(3) If the product were multimodal with no particles outside the size limits, the accuracy of the mass fractions would depend on the separation of the modes. The closer the modes, the more accurate the mass fractions. Further, the mass fractions of large particle seem to be exaggerated in the measurement.(4) If the product were multimodal with one or more modes of particles smaller than the lower limit on size (1.2 μm for the 63 mm lens), the mass fractions measured would be inaccurate. At low mass fractions of the undersize particles, the larger size particle mass fractions would be exaggerated. As the concentration of undersize particle increases, the measured mass fraction of oversize particles will fall below the actual level. The exact dependence is a function of the sizes of undersize and oversize particles.

The major cause of these problems is the coarse resolution (31 detector elements) used by the diffraction instrument to discretize the diffraction pattern. The use of a detector system with a larger number of elements will proportionally increase the resolution of the size distribution and make the sizing of multimodal distributions more accurate. Further, the simultaneous use of more than one Fourier lens greatly extends the size range analyzable in one sampling of the diffraction pattern. Both these features are present on instruments manufactured by other vendors. A study of the errors in these instruments is the subject of a future paper.

References

Swithenbank, J., Beer, J., Taylor, D.S., Abbott, D. and McCreath, C.O., In Zinn, B.T. (Ed.), Experimental diagnostics in gas-phase combustion systems: AIAA progress in astronautics and aeronautics, *AIAA* 53 (1977) 421.

Hirleman, E.D., Oechsle, V. and Chigier, N.A., *Opt. Eng.*, 23(5) (1984) 610

Bayvel, L. and Jones, A.R., *Electromagnetic Scattering and Applications*, Applied Science Publishers, London, 1981.

Gulari, E., Annapragada, A., Gulari, E. and Jawad, B., Particle size distribution: assessment and characterization, *ACS Symp. Ser.*, 332 (1985) 133.